Available online at www.sciencedirect.com

ScienceDirect

Journal of the European Ceramic Society 35 (2015) 1209–1217

www.elsevier.com/locate/jeurceramsoc

Stress-dependent electromechanical properties of doped $(Ba_{1-x}Ca_x)(Zr_yTi_{1-y})O_3$

Heide I. Humburg [a], Matias Acosta [a], Wook Jo [a,b], Kyle G. Webber [a,*], Jürgen Rödel [a]

[a] *Institute of Materials Science, Technische Universität Darmstadt, 64287 Darmstadt, Germany*

[b] *School of Materials Science and Engineering, Ulsan National Institute of Science and Technology, 689-798 Ulsan, Republic of Korea*

Received 3 July 2014; received in revised form 13 October 2014; accepted 15 October 2014

Available online 15 November 2014

Abstract

The effect of 1 at% Fe- and FeNb-doping on the temperature and stress stability of the electromechanical properties of $(Ba_{1-x}Ca_x)(Zr_yTi_{1-y})O_3$ (BCZT) was investigated. For the composition $(Ba_{0.89}Ca_{0.11})(Zr_{0.135}Ti_{0.865})O_3$ with rhombohedral symmetry, doping reduces the Curie point and the temperature stability of the large-signal electromechanical properties significantly. The large-signal piezoelectric coefficient d^*_{33} at room temperature was reduced to 500 pm/V compared to 700 pm/V in the undoped composition at 1 kV/mm. The electrostrain, however, was found to be less sensitive to mechanical prestresses, showing a plateau up to stresses of 80 MPa in both doped compositions. These effects were attributed to a reduction of the domain wall mobility due to a smaller grain size, charged defect dipoles and the proximity of the room-temperature measurements to the reduced ferroelectric-paraelectric phase transition temperature. The study reveals that the exceptionally large strains observed in BCZT rely on the instabilities around the polymorphic phase transition in the system. Aliovalent doping changes this sensitive system and reduces the electrostrain considerably.

Keywords: BZT-BCT; Doping; Piezoelectric properties; Lead-free; Ferroelasticity

1. Introduction

Piezoelectric materials are used in many applications, such as sensors, actuators and transducers. For actuators and high-precision positioning systems, a large recoverable electrostrain within a certain temperature regime at accessible driving field amplitudes is of primary importance. The large-signal piezoelectric coefficient d^*_{33}, defined as unipolar strain divided by the applied field, S/E, is the related figure of merit. Furthermore, stress and temperature stability are crucial properties, since multilayer actuators are commonly utilized under a compressive stress of 10–20 MPa to reduce the tendency to cracking, and frequently heat up during service.[1,2] These and other requirements are met by the ferroelectric system lead zirconate titanate $Pb(Zr_{1-x}Ti_x)O_3$ (PZT), which has dominated the actuator market over the past 60 years and currently holds 98% of the market share.[3] However, due to toxicity and environmental concerns, PZT is facing global restrictions in its usage in electronic equipment.[3–5] Therefore, there is an urgent need to develop Pb-free piezoelectric materials that can replace lead-containing ferroelectrics in actuation applications, particularly donor-doped PZT.

In 2009, Liu and Ren[6] reported the lead-free barium calcium zirconate titanate $(BaZr_{0.2}Ti_{0.8}O_3)-x(Ba_{0.7}Ca_{0.3}TiO_3)$ (BCZT) that featured piezoelectric constants on the order of 560–620 pm/V, clearly exceeding values for competing lead-free compositions and even those for most PZT materials.[3,7,8] In a narrow temperature window, the composition $(Ba_{0.85}Ca_{0.15})(Zr_{0.1}Ti_{0.9})O_3$ ($x = 50$ mol%) also exhibited an exceptionally large signal piezoelectric coefficient $d^*_{33} = 1140$ pm/V with an applied electric field of 0.5 kV/mm.[6] These large electromechanical properties were found to occur in a narrow temperature and compositional range in the vicinity of a temperature-dependent polymorphic phase transition (PPT). It was proposed that a coexistence of rhombohedral and tetragonal phases[9,10] lead to a flattening of the energy surface around

* Corresponding author. Tel.: +49 6151 16 6319.
E-mail address: webber@ceramics.tu-darmstadt.de (K.G. Webber).

http://dx.doi.org/10.1016/j.jeurceramsoc.2014.10.016
0955-2219/

the PPT, which is responsible for the enhanced properties. Following investigations have suggested, however, that the mixed phase region is an intermediate orthorhombic phase.[11,12] This results in high piezoelectric and electromechanical properties due to polarization rotation.[13] Nevertheless, more recent studies proposed that intrinsic and extrinsic properties can be analyzed separately.[14] It was suggested that polarization rotation and extension do play a role in the convergence region and at the PPT. Extrinsic contributions peaking around the PPTs were attributed to a broad minimum in switching energy barrier[14,15] leading to enhanced ferroelastic switching.[16]

Owing to its high electromechanical properties and high blocking stresses,[17] the BCZT system is a potential candidate for actuator applications. However, the system demonstrates a low Curie point[6] and a significant sensitivity of the small signal properties to mechanical prestress[18] and temperature,[19] which limits its applicability to conditions near room-temperature.[20]

Doping is a common strategy to alter the sensitivity of a material to external stimuli and optimize it for specific applications.[21,22] Only limited research exists on the effect of aliovalent doping on BCZT.[23–25] Due to the electrical hardening effect observed in doped $BaTiO_3$,[26,27] acceptor and acceptor–donor co-doping are effective approaches to enhance the stability of the electromechanical properties.[28,29] Typical aliovalent dopants in PZT are Nb^{5+} and Fe^{3+}, acting as donor and acceptor, respectively, which significantly alter the domain stability.[30] However, the influence of these additives on BCZT is not yet investigated. The aim of this work is, therefore, to characterize the effect of Fe^{3+} and Fe^{3+}/Nb^{5+} doping on the large-field electromechanical properties of BCZT. In particular, the influence of temperature and stress on the undoped, acceptor and co-doped BCZT is analyzed and compared.

2. Experimental procedure

Three compositions based on $(Ba_{0.865}Ca_{0.135})(Zr_{0.11}Ti_{0.89})O_3$ ($BC_{13.5}Z_{11}T$) (corresponds to $x = 45$ in BZT-xBCT) with different B-site dopants were prepared. The Ti and Zr-cations were replaced by 1 at% Fe [$(Ba_{0.865}Ca_{0.135})(Zr_{0.1089}Ti_{0.8811}Fe_{0.01})O_3$ (BCZT-*Fe*)] for acceptor doping and 1 at% of Fe and Nb each [$(Ba_{0.865}Ca_{0.135})(Zr_{0.1078}Ti_{0.8722}Fe_{0.01}Nb_{0.01})O_3$ (BCZT-*FeNb*)] for co-doping. The ceramics were prepared by a mixed oxide route using $BaCO_3$ (99.8%), $CaCO_3$ (99.5%), ZrO_2 (99.5%), TiO_2 (99.6%), Fe_2O_3 (99.5%) and Nb_2O_5 (99.9%) as raw materials (Alfa Aesar, Karlsruhe, Germany). The materials were weighed according to the stoichiometric formula and ball-milled for 5 h at 250 rpm. The dried slurries were calcined at 1300 °C for 2 h and subsequently ball-milled for 15 h. To ensure process reproducibility, two batches of powders were prepared and compared. The processed powders were uniaxially pressed into disc-shape and cylindrical samples, further compacted in a cold isostatic press at 300 MPa and sintered in covered zirconia crucibles with atmospheric powders at 1500 °C for 2 h.

The disc-shape samples for dielectric and temperature dependent measurements were ground to approximately 500 μm thickness and silver paste electrodes were applied manually and burnt-in at 400 °C for 2 h. The samples for electromechanical characterization were machined to a cylindrical shape with a diameter of 5.8 ± 0.1 mm and a height of 6 ± 0.03 mm. They were annealed at 400 °C for 2 h to reduce residual stresses and the faces were subsequently sputtered with silver electrodes.

X-ray diffraction experiments (D8 Advance, Bruker Inc., Germany) were conducted with CuK_α radiation ($\lambda = 1.5406$ Å). An angular range from 20 to 80° with a step size of 0.05° was scanned. Density measurements were performed using the classical Archimedes method. For microstructural analysis, samples were re-polished with diamond paste and etched in hydrochloric acid with a few drops of hydrofluoric acid for 1 min. Micrographs were taken using an optical microscope (DM RM/E, Leica Microsystems GmbH, Wetzlar, Germany). The average grain size was determined by the mean intercept length method with a minimum of 200 grains measured on 3 different locations of the sample. Assuming isometric grain shape a numerical multiplication factor of 1.56 was applied.

The temperature and frequency dependent dielectric properties were measured on poled samples with a commercial broadband dielectric spectrometer equipped with a cryostat temperature control (Novocontrol Technologies, Hundsangen, Germany). Prior to testing, the samples were poled at 4 kV/mm for 10 min at room-temperature to ensure a stable and comparable poled state.[31] Measurements were conducted in a N_2-gas heated chamber with an input voltage of 1 V and frequencies of 10^2–10^5 Hz in the temperature range of −100 °C to 120 °C with a heating rate of 2 °C/min.

Large signal unipolar and bipolar strain measurements were conducted at room-temperature with a triangular input field of 3 kV/mm and 5 Hz in a custom-built optical setup using a modified Sawyer-Tower circuit. Additional bipolar measurements were performed as a function of temperature using the commercial piezoelectric evaluation system TFAnalyzer 2000 E (aixPES, aixACCT Systems GmbH, Aachen, Germany). Large signal bipolar strain and polarization hysteresis loops were recorded at 25, 35, 45, 55, 65, 75, 85, 95 and 105 °C ($f = 5$ Hz, $E = 3$ kV/mm). Before each measurement step, the samples were held at the desired temperature for 5 min to ensure homogeneous heat distribution.

The mechanical stress dependent experiments were carried out using a Zwick Roell Z010 load frame with a customized sample environment that allows the simultaneous application of compressive mechanical stresses and electric fields. The sample holder was enclosed in a heating chamber with a thermocouple in the base of the sample mount that allows for temperature dependent measurements with a resolution of approximately ± 0.1 °C. The experimental setup and the reproducibility of measurements is presented in detail elsewhere.[32] Electric fields were applied using an Agilent 33220 arbitrary waveform generator connected to a TREK 20/20C high voltage power supply. The strain was measured using a linear variable differential transformer (LVDT) located well outside of the heated region. Unipolar strain and polarization were measured at room temperature, 50, 75 and 100 °C for 16 compressive stress values ranging from 2 MPa to 200 MPa. In the following discussion all stresses are compressive. At each mechanical load the sample

Table 1
Average relative density, grain size and summary of characteristic properties extracted from bipolar polarization and strain and unipolar strain measurements for all compositions.

	ρ_r %	Grain size µm	E_c kV/mm	P_r µC/cm^2	S_r %	d^*_{33} [a]
$BC_{13.5}Z_{11}T$	97 ± 0	22 ± 3	0.31	9.8	0.023	690
BCZT-*Fe*	97 ± 1	12 ± 1	0.17	2.4	0.002	490
BCZT-*FeNb*	98 ± 0	10 ± 1	0.19	3.8	0.002	500

[a] Measured at an electric field of 1 kV/mm.

was cycled at a frequency of 0.05 Hz with two unipolar cycles of 3, 2 and 1 kV/mm, respectively. The second cycle of each field amplitude was used for evaluation. After mounting the sample into the setup, a prestress of 2 MPa was applied to ensure contact. The sample was held at the desired temperature for 15 min to ensure thermal equilibrium. Subsequently, five poling cycles with 3 kV/mm at 0.05 Hz were applied. The stress was kept constant during electrical cycling with a force-control rate of 100 N/s. After the largest stress, the measurement at 2 MPa was repeated to exclude the possibility of electric fatigue. No difference was observed between the first measurement and the one after mechanical loading.

3. Results & discussion

3.1. General characterization

The structural analysis of the three compositions $BC_{13.5}Z_{11}T$, BCZT-*Fe* and BCZT-*FeNb* reveals relative densities between 97 and 98% and large differences in grain size (Table 1).

Doping reduces the grain size significantly from 22 µm in $BC_{13.5}Z_{11}T$ to 12 and 10 µm in BCZT-*Fe* and BCZT-*FeNb*, respectively.

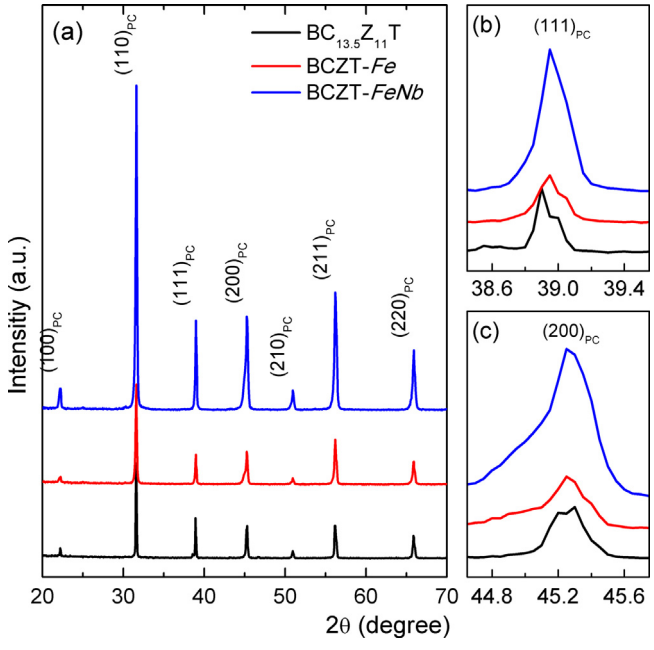

Fig. 1. X-ray diffraction patterns of sintered samples (a). The (1 1 1) and the (2 0 0) reflections are shown in (b) and (c).

The X-ray patterns are provided in (Fig. 1). All compositions demonstrate a phase-pure perovskite structure with pseudo-cubic (pc) symmetry (Fig. 1a). Non-cubic distortions cannot be detected in the doped compositions, while the pure $BC_{13.5}Z_{11}T$ displays peak splitting in the $(1\,1\,1)_{pc}$ and $(2\,0\,0)_{pc}$ reflections (Fig. 1b and c).

The results of the real part of the relative permittivity ε_r' and the loss factor *tan δ* as a function of temperature are provided in Fig. 2. As previously reported,[14] the local maxima of the *tan δ* could be utilized to detect phase transitions and matches the inflection of ε'_r at T_c.[14,33] Consistent with previous results,[9,10,34] $BC_{13.5}Z_{11}T$ demonstrates three distinct anomalies at 15 (T_1), 37 (T_2) and 74 °C (T_m) (Fig. 2a). The latter seems to correspond to the ferroelectric-paraelectric phase transition; the former two anomalies indicate the rhombohedral-orthorhombic (R-O) and orthorhombic-tetragonal (O-T) phase transitions.[11] As reported in previous works,[35,36] ε_r' is only weakly frequency-dependent. In comparison, the maximum permittivity $\varepsilon'_{r\,max}$ peak at T_m is

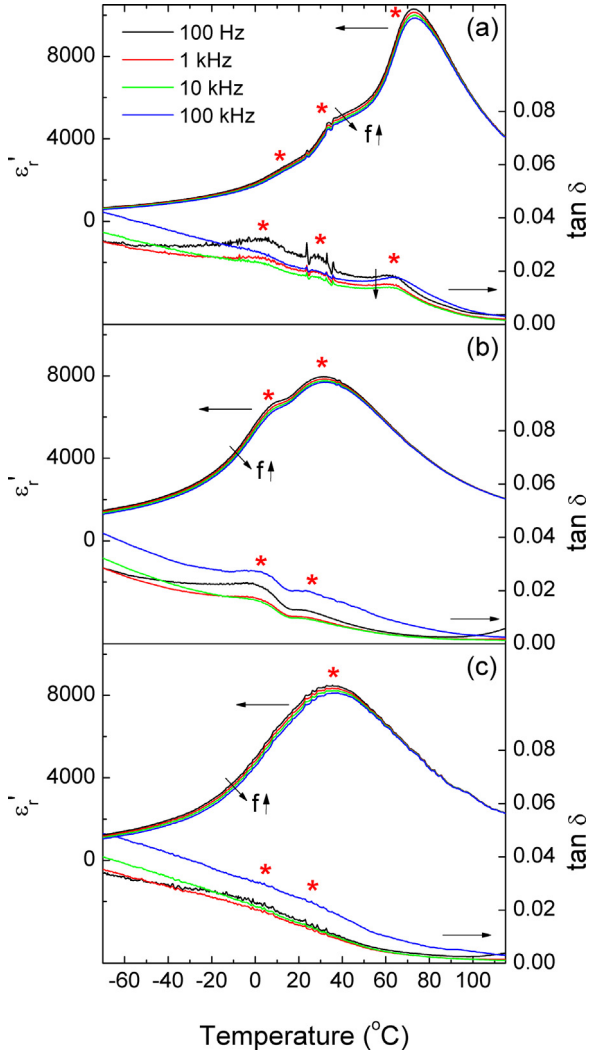

Fig. 2. Temperature dependent permittivity ε'_r and dielectric loss *tan δ* upon heating at 2 K/min. (a) $BC_{13.5}Z_{11}T$. (b) BCZT-*Fe*. (c) BCZT-*FeNb*. Arrows indicate increasing measurement frequency. Stars mark phase transition temperatures.

broadened and depressed in the doped compositions (Fig. 2b and c), in addition to occurring at significantly lower temperatures of 32 and 38 °C for BCZT-*Fe* and BCZT-*FeNb*, respectively. This corresponds to a decrease in T_m of around 40 °C with respect to the undoped composition. The three distinct phase transitions in $BC_{13.5}Z_{11}T$ are merged to two and one single discernible phase transition in BCZT-*Fe* and BCZT-*FeNb*, respectively. The T_m in the undoped material could be termed the Curie temperature T_c. Since doped materials present relaxor-like features and do not follow the Curie-Weiss law in the vicinity of maximum permittivity, T_m was used to denote the maximum relative permittivity value.

Bipolar and unipolar electric field-induced strain and polarization curves at room-temperature are presented in Fig. 3. The important parameters are listed in Table 1. The undoped composition displays significant remanent polarization (Fig. 3a) and strain (Fig. 3b) and a low coercive field of 0.31 kV/mm. Furthermore, the undoped composition exhibits a unipolar strain of 0.07% at 1 kV/mm, corresponding to a d^*_{33} of 690 pm/V (Fig. 3d). In contrast, BCZT-*Fe* and BCZT-*FeNb* display almost negligible, low P_r and, in contrast to observations made in hard doped PZT,[37] a lower E_c than $BC_{13.5}Z_{11}T$. The maximum unipolar strain is significantly lower, resulting in d^*_{33} of 490 and 500 pm/V at 1 kV/mm for the *Fe*-doped and the co-doped material, respectively. While the maximum bipolar polarization is lower for the doped compositions, the unipolar polarization P_{max} is higher due to the reduced remanent polarization (Fig. 3c). Additionally, the low E_c and a more tilted $P(E)$-loop result in lower hysteretic losses.

BCZT-*Fe* displays aging features typical for acceptor-doped materials,[28] illustrated by the pinched $P(E)$-loop (Fig. 3a) and a double peak in the switching current (Fig. 3B). These effects are not as pronounced in the co-doped material (Fig. 3C) and inexistent in $BC_{13.5}Z_{11}T$ (Fig. 3A). Aging in ferroelectrics is primarily related to oxygen vacancies forming defect dipoles with acceptor cations or charge accumulation at grain or domain boundaries. In either case, the mobility of domain walls is reduced.[28] In the "defect dipole" model the effect is explained by the stabilization of a certain domain configuration due to aligned defect dipoles.[38–40] The "domain wall" model on the other hand attributes the stabilization to the formation of space charges at domain walls or near grain boundaries.[41,42] Independent of the still disputed underlying mechanisms, aging reduces the domain wall mobility, hence lowering the extrinsic contribution to strain and the dielectric losses associated with domain wall displacement. Therefore, the reduced $\varepsilon'_{r\,max}$ and *tan δ* as well as the lower strain and hysteretic losses in the $P(E)$-loops in both doped compositions indicate a stabilization of domain walls. Assuming the defect dipole model, this can be attributed to aging due to the formation of charged defect complexes in the acceptor-doped material $(Fe_{Ti}{}'–V_O{}^{\bullet\bullet})^{\bullet}$. This stabilizes the ferroelectric properties and leads to an increase in $\varepsilon'_{r\,max}$, *tan δ* and T_m compared to acceptor doping.

Grain size is known to have significant effects on the dielectric and piezoelectric properties in BCZT.[36] With finer grain size, the mobility of the domain walls is reduced, which suppresses the Curie peak[23] and weakens the electromechanical properties in BCZT.[36] This corresponds well to the observations in the present investigation. However, with decreasing grain size an increase in T_m is expected.[36] The difference in the dielectric and electromechanical characteristics between $BC_{13.5}Z_{11}T$ and the doped compositions can, therefore, only be partially explained by the difference in grain size. Iron doping, on the other hand, is known to lower T_m by 40–75 °C per mol% of doping in BT,[22]

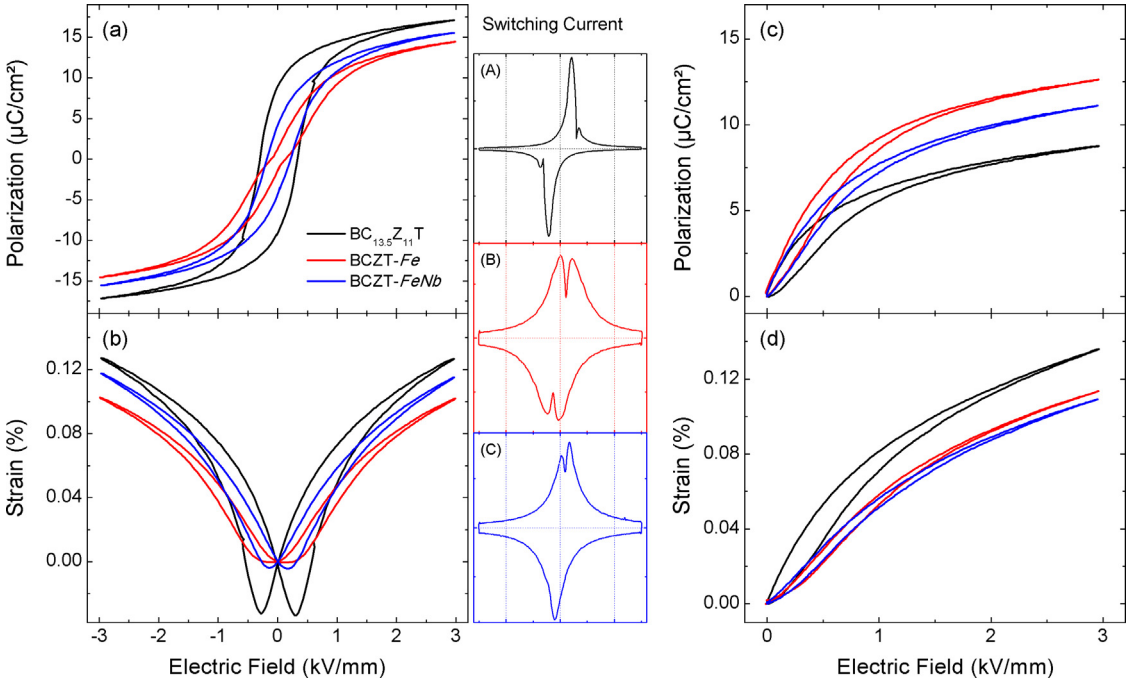

Fig. 3. Representative bipolar and unipolar polarization (a and c) and strain (b and d) versus electric field for all compositions. Subfigures A–C provide the switching current of the bipolar measurements. All measurements were conducted at room-temperature with a maximum field of 3 kV/mm at 5 Hz frequency.

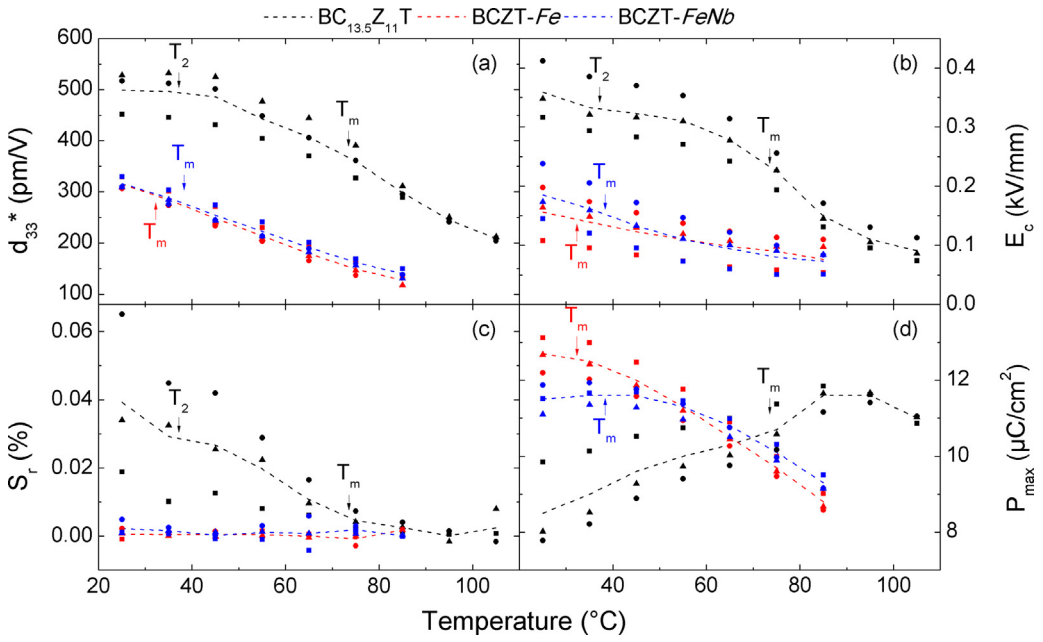

Fig. 4. (a) Large-signal piezoelectric coefficient d^*_{33} at 3 kV/mm, (b) coercive field E_c, (c) remanent strain S_r and (d) unipolar maximum polarization P_{max} as a function of temperature for all compositions. The dashed line represents the respective mean values. All measurements were conducted with $f = 5$ Hz. Marked are the phase transition temperatures T_m and T_2.

while co-doping partially eliminates this effect.[23] The former phenomenon is attributed to the influence of local compositional fluctuations and random charge and strain fields introduced by the aliovalent dopants that locally reduce the tetragonal symmetry and the ferroelectric state.[22,23] These features cause smeared phase transitions and generally reduce T_m significantly. They are also known to diminish remanent polarization, coercive field and remanent strain,[22] which matches the observed properties in the doped compositions. The effect of these general characteristics of the doped compositions on the temperature and stress-dependent electromechanical properties is evaluated in the following sections.

3.2. Temperature dependence

Characteristic parameters of the field-induced strain and polarization measurements conducted at different temperatures are provided in Fig. 4. The phase transitions obtained from dielectric properties (Fig. 2) in the temperature range of the electromechanical experiments are marked.

For $BC_{13.5}Z_{11}T$, d^*_{33} at 3 kV/mm displays less than 3% variation between 25 and 45 °C with approximately 495 pm/V (Fig. 4a). This plateau corresponds to the observed phase-transition temperature of 37 °C. The doped compositions do not show a plateau in d^*_{33} which decreases steadily with temperature. The coercive field is almost temperature-insensitive for $BC_{13.5}Z_{11}T$ up to 55 °C with an average value of 0.35 kV/mm. On crossing the ferroelectric-paraelectric phase transition at T_m, it is then reduced significantly to 0.15 kV/mm at 85 °C. For BCZT-*Fe* and BCZT-*FeNb* the coercive field displays maximum values of 0.18 and 0.2 kV/mm, respectively. It decreases monotonically with temperature giving an average value of 0.08 kV/mm at 85 °C (Fig. 4b). The remanent strain S_r decreases from 0.04% at room-temperature to zero at 85 °C for the undoped composition, while it remains around zero at all temperatures for the two doped compositions (Fig. 4c). A plateau in the attainable polarization P_{max} is observed between 25 and 55 °C for BCZT-*FeNb* and between 85 and 95 °C for $BC_{13.5}Z_{11}T$. For BCZT-*Fe* the maximum P_{max} is reached at room-temperature, after which it decreases monotonically with temperature (Fig. 4d). The maxima roughly correspond to the respective ferroelectric-paraelectric phase transition temperatures. It is expected that the high-field electrostrictive coefficient remains relatively constant with temperature in perovskite ferroelectrics.[43,44] Nevertheless, the experimental data indicates that the high-field electrostrictive coefficient gradually decreases with decreasing temperature. This is reflected as a gradual decrease in the strain (Fig. 4a) and increase in polarization (Fig. 4d). Similar behavior was observed in other BZT-BCT compositions.[14] This behavior is not currently understood.

Since the doped compositions display a significantly lower T_m, the temperature-dependent measurements are closer to the Curie point than for $BC_{13.5}Z_{11}T$. To evaluate the effect of doping apart from the shift in T_m, the properties at temperatures with equal distance to T_m are compared. Although the difference between the compositions is diminished, distinct characteristics are distinguishable. The large-signal piezoelectric coefficient d^*_{33} (Fig. 5), E_c and S_r are still significantly lower, while P_{max} is enhanced in the doped materials.

The reduced strain compared to the undoped material can be rationalized by the aforementioned defect induced electrical hardening effect, which reduces the extrinsic contribution to strain. A reduced long-range ferroelectric order due to random charge and strain fields on the other hand can explain the lower coercive field, remanent strain and

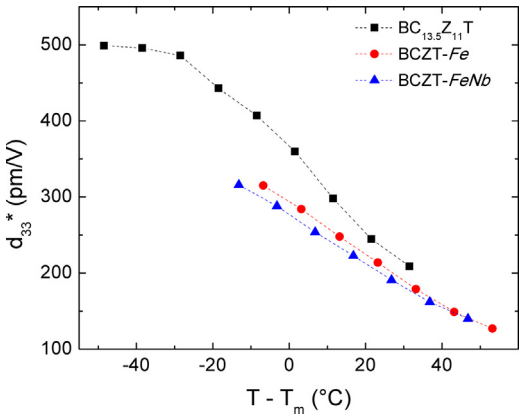

Fig. 5. Mean value of the large-signal piezoelectric coefficient d^*_{33} at 3 kV/mm as a function of the distance to T_m.

polarization even at temperatures with equivalent distance to T_m.

3.3. Stress-dependence

Fig. 6 provides select stress-dependent electric-field induced strain curves at different temperatures and fields for all compositions. At the minimum stress level (2 MPa) the features of the stress-free measurements are reproduced (see Fig. 3d). However, at moderate stress, hysteresis and strain increase in $BC_{13.5}Z_{11}T$ (Fig. 6a) at 25 and 50 °C for all electric field levels (as reported before by Ehmke et al. [20]) and then gradually diminish at higher stresses. The threshold field required to initiate unipolar strain and to overcome mechanical domain clamping increases with stress. In contrast, doped materials display less hysteresis and a less pronounced effect of stress on electric field induced strain (Fig. 6b and c). All compositions show electrostrictive behavior above T_m.

The evolution of d^*_{33} under stress for different temperatures is provided in Fig. 7. In the undoped material (Fig. 7a) the highest d^*_{33} at 2 MPa is found at 1 kV/mm for all temperatures. In the doped compositions the same observation holds true only at 25 °C which is due to the lower ferroelectric-paraelectric transition temperature. In $BC_{13.5}Z_{11}T$, d^*_{33} peaks at moderate stress levels, σ_{peak}, of 15 MPa with 800 pm/V (1 kV/mm). For higher field amplitudes lower maxima are observed and σ_{peak} is shifted to higher stress values of 25 MPa (2 kV/mm) and 40 MPa (3 kV/mm). The stress dependence is higher at low fields. As an illustration, d^*_{33} at 60 MPa decreased by 42% compared to the initial preload stress value for 1 kV/mm, while it increases by 3% for 2 kV/mm and 6% for 3 kV/mm.

For BCZT-*Fe* (Fig. 7b) and BCZT-*FeNb* (Fig. 7c), d^*_{33} is lower but more stable with stress. No distinct peaks can be observed in d^*_{33} with increasing compressive stress. Instead, d^*_{33} shows a plateau region at room-temperature up to approximately 60 MPa, depending on the actuation field. The maximum values do not exceed 400 and 450 pm/V at 1 kV/mm in BCZT-*Fe* and BCZT-*FeNb*, respectively. Consistent with the previous measurements (see Fig. 4), the d^*_{33} presents a large temperature dependence in all compositions. In $BC_{13.5}Z_{11}T$, the stress at maximum d^*_{33}

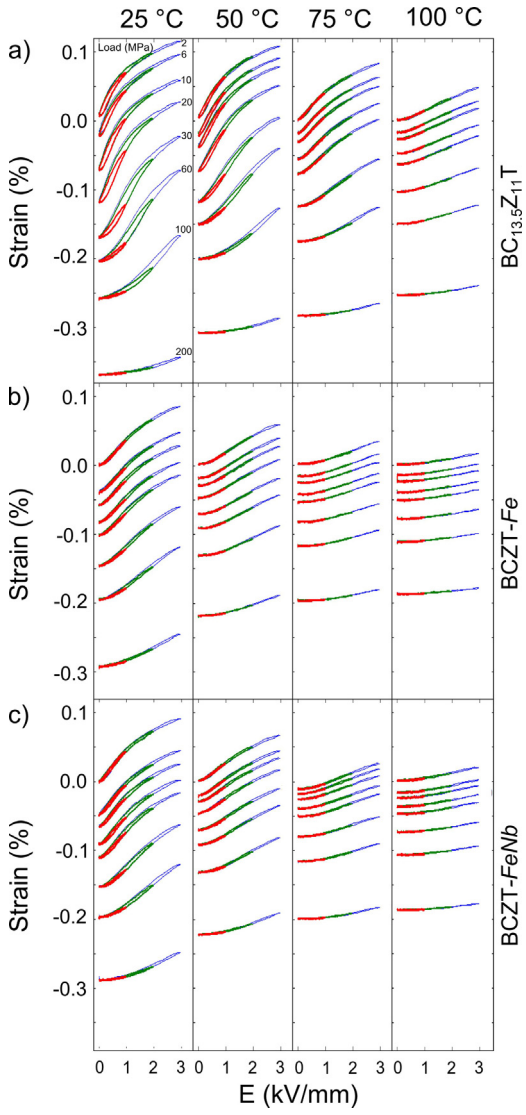

Fig. 6. Unipolar field-induced strain of all compositions for selected compressive stresses (2, 6, 10, 20, 30, 60, 100, 200 MPa) at temperatures ranging from 25 °C to 100 °C (left to right) at 1 kV/mm (red), 2 kV/mm (green) and 3 kV/mm (blue) for (a) BCZT, (b) BCZT-*Fe* and (c) BCZT-*FeNb*. (For interpretation of the references to color in this figure legend, the reader is referred to the web version of the article.)

shifts to lower values at 50 °C and is not discernible at 75 °C. A stable but very low d^*_{33} is observable at temperatures exceeding the respective T_m for all compositions.

The initial increase in d^*_{33} at moderate stress levels can be rationalized with the in-plane alignment of domains under stress. These additional non-180° domains can be reoriented in electric field direction at sufficiently large electric fields and contribute to the macroscopic strain. At higher stresses, the domains become mechanically clamped perpendicular to the field direction; the electric field is insufficient to overcome the applied stress and the extrinsic contribution to the macroscopic strain is reduced. This behavior was observed by Chaplya and Carman[45] for PZT and confirmed by several studies, *e.g.* by Kerkamm et al.[46] in PZT multilayers and Dittmer et al.[47] in BNT-6BT. At 2 kV/mm the maximum d^*_{33} is reached

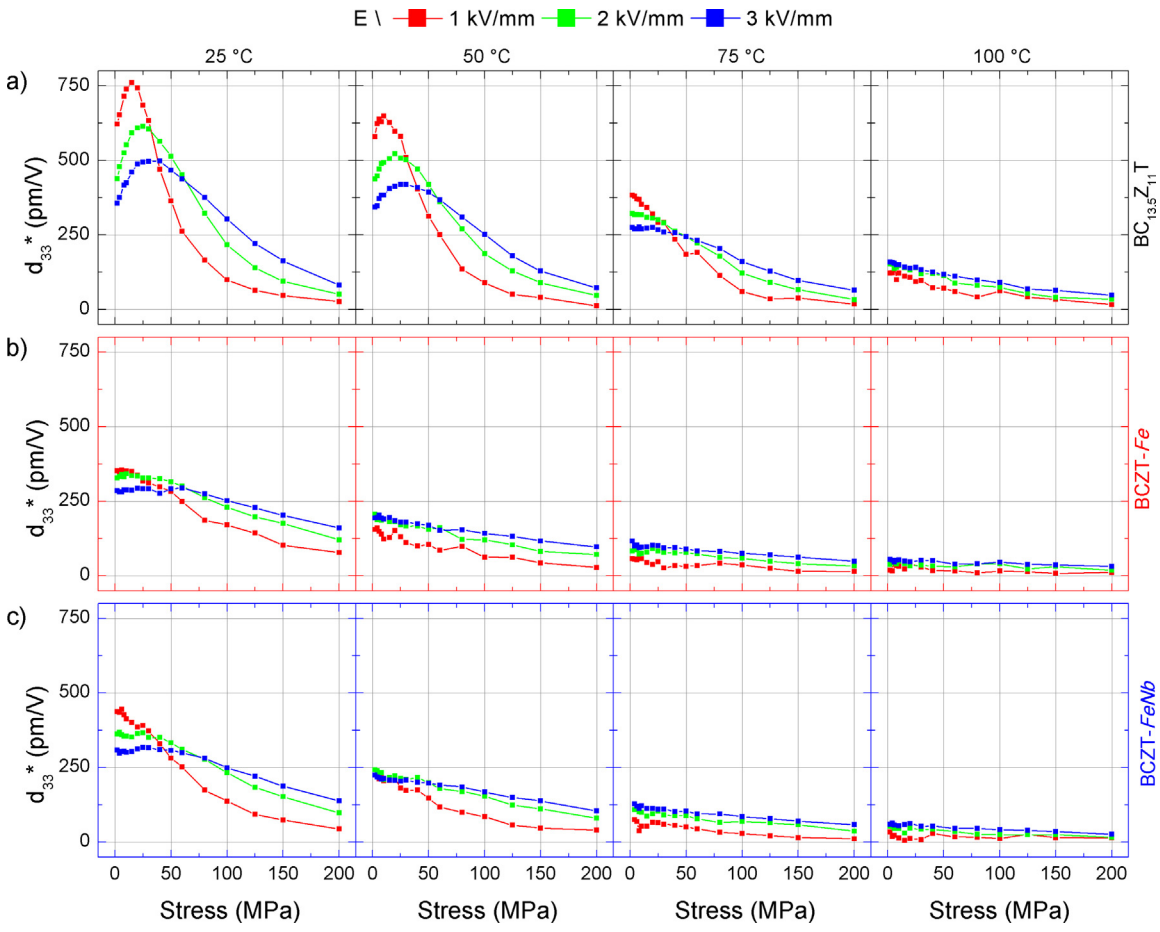

Fig. 7. The d^*_{33} as a function of stress for different field amplitudes and temperatures (left to right). (a) $BC_{13.5}Z_{11}T$. (b) BCZT-*Fe*. (c) BCZT-*FeNb*.

at 50 MPa in soft PZT,[45] which also corresponds to its critical stress for ferroelastic switching.[32] The effect is less pronounced in $BC_{13.5}Z_{11}T$ and, with $\sigma_{peak} = 25$ MPa, occurs and saturates at lower stresses than in PZT. Although ferroelastic measurements of the same compositions have not been conducted yet, results on similar compositions also indicate a lower critical stress of 10–25 MPa.[17,20] Nevertheless, the same mechanisms as in PZT are responsible for the observed peak in d^*_{33}. These results confirm that moderate stresses in $BC_{13.5}Z_{11}T$ can enhance the electrostrain considerably.

Hard doping in PZT leads to a higher critical onset stress for ferroelastic switching.[37] Correspondingly, a maximum in d^*_{33} would be expected at higher stress in BCZT-*Fe* than in the undoped composition. It was observed, however, that the non-180° domain switching is clamped to a large extent even at low stresses and a stress-dependent enhancement of d^*_{33} cannot be observed. Additionally, the missing peak in d^*_{33} in the doped compositions indicates a lower ferroelastic switching contribution to the overall strain. A lower tetragonality of the unit cell close to T_m could be responsible for this phenomenon, making both doped composition less sensitive to compressive stress. Furthermore, the stress-dependent d^*_{33} in the undoped composition at 75 °C reveals strong similarity to the room-temperature results of the doped compositions. This observation strongly indicates that the proximity to the ferroelectric-paraelectric phase transition temperature is an important factor determining the response of the material, in agreement to electromechanical properties previously reported.[14] The comparison of the stress-free d^*_{33} as a function of distance to T_m (Fig. 5), however, demonstrates that doping still has an effect on the electrostrain. Similar stress-dependent measurements could give further insight into the mechanisms controlling the electromechanical properties of doped BCZT.

4. Conclusions

Doping in $(Ba_{0.865}Ca_{0.135})(Zr_{0.11}Ti_{0.89})O_3$ ($BC_{13.5}Z_{11}T$) was found to have strong effects on microstructure, dielectric and electromechanical properties. The main effects of Fe- and Fe/Nb co-doping are (i) a reduction of the grain size, (ii) a significantly lower ferroelectric-paraelectric phase transition temperature close to room-temperature, (iii) a slightly pinched $P(E)$-loop and a double peak in the switching current of the acceptor doped material and (iv) a reduction of d^*_{33} as a function of temperature and stress, which can mainly be attributed to the change in the phase transition temperature. The investigations confirm that the exceptionally large strains observed in BCZT rely on the instabilities around the polymorphic phase transition in the system. Aliovalent doping changes this sensitive system and reduces the electrostrain considerably.

Acknowledgements

This work was financially supported by the state center AdRIA on adaptronics. K.G.W. gratefully acknowledges financial support for his contributions from the Deutsche Forschungsgemeinschaft under WE4972/2-1.

References

1. Randall CA, Kelnberger A, Yang GY, Eitel RE, Shrout TR. High strain piezoelectric multilayer actuators-a material science and engineering challenge. *J Electroceram* 2005;**14**:177.
2. Senousy MS, Rajapakse RKND, Mumford D, Gadala MS. Self-heat generation in piezoelectric stack actuators used in fuel injectors. *Smart Mater Struct* 2009;**18**:045008.
3. Jo W, Dittmer R, Acosta M, Zang J, Groh C, Sapper E, et al. Giant electric-field-induced strains in lead-free ceramics for actuator applications - status and perspective. *J Electroceram* 2012;**29**:71.
4. EU-Directive. Waste electrical and electronic equipment (WEEE). 2002/96/EC. *Off J Eur Union* 2003;**46**:24.
5. EU-Directive. The restriction of the use of certain hazardous substances in electrical and electronic equipment (RoHS). 2011/65/EU. *Off J Eur Union* 2011;**L174**:88.
6. Liu WF, Ren XB. Large piezoelectric effect in Pb-free ceramics. *Phys Rev Lett* 2009;**103**:257602.
7. Rödel J, Jo W, Seifert KTP, Anton E-M, Granzow T, Damjanovic D. Perspective on the development of lead-free piezoceramics. *J Am Ceram Soc* 2009;**92**:1153.
8. Shrout TR, Zhang SJ. Lead-free piezoelectric ceramics: alternatives for PZT? *J Electroceram* 2007;**19**:113.
9. Ehmke MC, Ehrlich SN, Blendell JE, Bowman KJ. Phase coexistence and ferroelastic texture in high strain $(1-x)$Ba(Zr0.2Ti0.8)O3$-x$(Ba0.7Ca0.3)TiO_3 piezoceramics. *J Appl Phys* 2012;**111**:124110.
10. Haugen AB, Forrester JS, Damjanovic D, Li B, Bowman KJ, Jones JL. Structure and phase transitions in 0.5(Ba0.7Ca0.3TiO_3)-0.5(BaZr0.2Ti0.8O_3) from −100 °C to 150 °C. *J Appl Phys* 2013;**113**:014103.
11. Keeble DS, Benabdallah F, Thomas PA, Maglione M, Kreisel J. Revised structural phase diagram of (Ba0.7Ca0.3TiO_3)-(BaZr0.2Ti0.8O_3). *Appl Phys Lett* 2013;**102**:092903.
12. Tian Y, Wei L, Chao X, Liu Z, Yang Z. Phase transition behavior and large piezoelectricity near the morphotropic phase boundary of lead-free (Ba0.85Ca0.15)(Zr0.1Ti0.9)O_3 ceramics. *J Am Ceram Soc* 2013;**96**:496.
13. Damjanovic D. A morphotropic phase boundary system based on polarization rotation and polarization extension. *Appl Phys Lett* 2010;**97**:062906.
14. Acosta M, Novak N, Jo W, Rödel J. Relationship between electromechanical properties and phase diagram in the Ba(Zr0.2Ti0.8)O_3-x(Ba0.7Ca0.3)TiO_3 lead-free piezoceramic. *Acta Mater* 2014;**80**:48.
15. Zhukov S, Genenko YA, Acosta M, Humburg H, Jo W, Rödel J, et al. Polarization dynamics across the morphotropic phase boundary in Ba(Zr0.2Ti0.8)O_3-x(Ba0.7Ca0.3)TiO_3 ferroelectrics. *Appl Phys Lett* 2013;**103**:152904.
16. Tutuncu G, Li B, Bowman K, Jones JL. Domain wall motion and electromechanical strain in lead-free piezoelectrics: Insight from the model system $(1-x)$Ba(Zr0.2Ti0.8)O3–x(Ba0.7Ca0.3)TiO_3 using in situ high-energy X-ray diffraction during application of electric fields. *J App Phys* 2014;**115**:144104.
17. Brandt DRJ, Acosta M, Koruza J, Webber KG. Mechanical constitutive behavior and exceptional blocking force of lead-free BZT-BCT piezoceramics. *J App Phys* 2014;**115**:204107.
18. Ehmke MC, Daniels J, Glaum J, Hoffman M, Blendell JE, Bowman KJ. Reduction of the piezoelectric performance in lead-free $(1-x)$Ba(Zr0.2Ti0.8)O_3-x(Ba0.7Ca0.3)TiO_3 piezoceramics under uniaxial compressive stress. *J Appl Phys* 2012;**112**:114108.
19. Xue DZ, Zhou YM, Bao HX, Zhou C, Gao JH, Ren XB. Elastic, piezoelectric, and dielectric properties of Ba(Zr0.2Ti0.8)O_3-50(Ba0.7Ca0.3)TiO_3 Pb-free ceramic at the morphotropic phase boundary. *J Appl Phys* 2011;**109**:054110.
20. Ehmke MC, Schader FH, Webber KG, Rödel J, Blendell JE, Bowman KJ. Stress, temperature and electric field effects in the lead-free (Ba,Ca)(Ti Zr)O3 piezoelectric system. *Acta Mater* 2014;**78**:37.
21. Cao W. Defects in ferroelectrics. *Springer Ser Mater Sci Springer Berlin Heidelberg* 2012;**148**:113.
22. Jaffe B, Cook WR, Jaffe HL. *Piezoelectric ceramics*. London: Academic Press; 1971.
23. Hansen P, Hennings D, Schreinemacher H. Dielectric properties of acceptor-doped (Ba,Ca)(Ti,Zr)O_3 ceramics. *J Electroceram* 1998;**2**:85.
24. Li W, Xu Z, Chu R, Fu P, Zang G. Temperature stability in Dy-doped (Ba0.99Ca0.01)(Ti0.98Zr0.02)O_3 lead-free ceramics with high piezoelectric coefficient. *J Am Ceram Soc* 2011;**94**:3181.
25. Li W, Xu Z, Chu R, Fu P, Zang G. High piezoelectric d33 coefficient of lead-free (Ba0.93Ca0.07)(Ti0.95Zr0.05)O_3 ceramics sintered at optimal temperature. *Mater Sci Eng B Adv* 2011;**176**:65.
26. Hagemann HJ. Loss mechanisms and domain stabilisation in doped $BaTiO_3$. *J Phys C: Solid State Phys* 1978;**11**:3333.
27. Unruan M, Sareein T, Tangsritrakul J, Prasertpalichatr S, Ngamjarurojana A, Ananta S, et al. Changes in dielectric and ferroelectric properties of Fe^{3+}/Nb^{5+} hybrid-doped barium titanate ceramics under compressive stress. *J Appl Phys* 2008;**104**:124102.
28. Carl K, Härdtl KH. Electrical after-effects in Pb(Ti, Zr)O_3 ceramics. *Ferroelectrics* 1978;**17**:473.
29. Takahashi S. Effects of impurity doping in lead zirconate-titanate ceramics. *Ferroelectrics* 1982;**41**:143.
30. Haertling GH. Ferroelectric Ceramics: History and Technology. *J Am Ceram Soc* 1999;**82**:797.
31. Wu JG, Xiao DQ, Wu WJ, Chen Q, Zhu JG, Yang ZC, et al. Composition and poling condition-induced electrical behavior of (Ba0.85Ca0.15)(Ti1-xZrx)O_3 lead-free piezoelectric ceramics. *J Eur Ceram Soc* 2012;**32**:891.
32. Webber KG, Aulbach E, Key T, Marsilius M, Granzow T, Rödel J. Temperature-dependent ferroelastic switching of soft lead zirconate titanate. *Acta Mater* 2009;**57**:4614.
33. Bhaumik I, Singh G, Ganesamoorthy S, Bhatt R, Karnal AK, Tiwari VS, et al. Growth of lead-free piezoelectric 0.45BZT–0.55BCT single crystal and investigation of dielectric, polarization and birefringence properties. *J Cryst Growth* 2013;**375**:20.
34. Damjanovic D, Biancoli A, Batooli L, Vahabzadeh A, Trodahl J. Elastic, dielectric, and piezoelectric anomalies and Raman spectroscopy of 0.5 Ba($Zr_{0.2}Ti_{0.8}$)O_3–0.5($Ba_{0.7}Ca_{0.3}$)TiO_3. *Appl Phys Lett* 2012;**100**:192907.
35. Su S, Zuo R, Lu S, Xu Z, Wang X, Li L. Poling dependence and stability of piezoelectric properties of Ba($Zr_{0.2}Ti_{0.8}$)O_3–($Ba_{0.7}Ca_{0.3}$)TiO_3 ceramics with huge piezoelectric coefficients. *Curr Appl Phys* 2011;**11**:120.
36. Hao J, Bai W, Li W, Zhai J. Correlation between the microstructure and electrical properties in high-performance ($Ba_{0.85}Ca_{0.15}$)($Zr_{0.1}Ti_{0.9}$)O_3 lead-free piezoelectric ceramics. *J Am Ceram Soc* 2012;**95**:1998.
37. Cao H, Evans AG. Nonlinear deformation of ferroelectric ceramics. *J Am Ceram Soc* 1993;**76**:890.
38. Arlt G, Neumann H. Internal bias in ferroelectric ceramics: origin and time dependence. *Ferroelectrics* 1988;**87**:109.
39. Robels U, Arlt G. Domain wall clamping in ferroelectrics by orientation of defects. *J Appl Phys* 1993;**73**:3454.
40. Eichel R-A, Erhart P, Träskelin P, Albe K, Kungl H, Hoffmann MJ. Defect-dipole formation in copper-doped $PbTiO_3$ ferroelectrics. *Phys Rev Lett* 2008;**100**:095504.
41. Thomann H. Stabilization effects in piezoelectric lead titanate zirconate ceramics. *Ferroelectrics* 1972;**4**:141.
42. Genenko YA, Glaum J, Hirsch O, Kungl H, Hoffmann MJ, Granzow T. Aging of poled ferroelectric ceramics due to relaxation of random depolarization fields by space-charge accumulation near grain boundaries. *Phys Rev B* 2009;**80**:224109.

43. Dittmer R, Webber KG, Aulbach E, Jo W, Tan X, Rödel J. Optimal working regime of lead-zirconate-titanate for actuation applications. *Sens Actuator A Phys* 2013;**189**:187.
44. Weaver PM, Cain MG, Stewart M. Temperature dependence of high field electromechanical coupling in ferroelectric ceramics. *J Phys D: Appl Phys* 2010;**43**:165404.
45. Chaplya PM, Carman GP. Dielectric and piezoelectric response of lead zirconate-lead titanate at high electric and mechanical loads in terms of non-180° domain wall motion. *J Appl Phys* 2001;**90**: 5278.
46. Kerkamm I, Hiller P, Granzow T, Rödel J. Correlation of small- and large-signal properties of lead zirconate titanate multilayer actuators. *Acta Mater* 2009;**57**:77.
47. Dittmer R, Webber KG, Aulbach E, Jo W, Tan X, Rödel J. Electric-field-induced polarization and strain in $0.94(Bi1/2Na1/2)TiO_3-0.06BaTiO_3$ under uniaxial stress. *Acta Mater* 2013;**61**:1350.